# Iterative CT Reconstruction Using Curvelet-Based Regularization

Haibo Wu[1,2], Andreas Maier[1], Joachim Hornegger[1,2]

[1]Pattern Recognition Lab (LME), Department of Computer Science,
[2]Graduate School in Advanced Optical Technologies (SAOT),
Friedrich-Alexander-University Erlangen-Nuremberg
haibo.wu@informatik.uni-erlangen.de

**Abstract.** There is a critical need to reconstruct clinically usable images at a low dose. One way of achieving this is to reconstruct with as few projections as possible. Due to the undersampling, streak artifacts degrade image quality for traditional CT reconstruction. Compressed sensing (CS) [1] theory uses sparsity as a prior and improves the reconstruction quality considerably using only few projections. CS formulates the reconstruction problem to an optimization problem. The objective function consists of one data fidelity term and one regularization term which enforce the sparsity under a certain sparsifying transform. Curvelet is an effective sparse representation for objects [2]. In this work, we introduce to use curvelet as the sparsifying transform in the CS based reconstruction framework. The algorithm was evaluated with one physical phantom dataset and one in vitro dataset and was compared against and two state-of-art approach, namely, wavelet-based regularization (WR) [3] and total variation based regularization methods (TVR) [4]. The results show that the reconstruction quality of our approach is superior to the reconstruction quality of WR and TVR.

## 1 Introduction

Computed tomography is used as a common examination tool in diagnosis and interventional procedures. However, increasing concerns about radiation exposure have been raised in recent years [5]. Recently, compressed sensing (CS) theory has been introduced [1]. CS asserts that the signal sampling rate which guarantees accurate reconstruction is proportional to the complexity of signal rather than its dimensionality. Most natural signals are well described by only a few significant coefficients in some domain, where the number of significant coefficients is much smaller than the signal size on an equally spaced grid. As such, the signals that are sparse or compressible can be recovered from very few measurements. Several CS based CT reconstruction algorithms have been proposed [3, 4, 6]. It has been found in these papers that the number of x-ray projections can be significantly reduced with little sacrifice in CT image quality. Thus, CS based reconstruction algorithm can reduce the radiation dose under the assumption that the dose is proportional to the number of x-ray projections.

H.-P. Meinzer et al. (Hrsg.), *Bildverarbeitung für die Medizin 2013*, Informatik aktuell,
DOI: 10.1007/978-3-642-36480-8_41, 

A proper sparsifying transform is critical for CS based reconstruction methods. Recently, Candes, who proposed the CS theory, designed a efficient sparsifying transform which is called curvelet [2, 7]. The curvelet transform is a multi scale pyramid with many directions and positions at each length scale, and needle-shaped elements at fine scales. One feature of curvelet makes it very suitable for CS based reconstruction method. Let $f_m$ be the $m$-term curvelet approximation to the object $f$, in other words, to represent object $f$ using $m$ largest curvelet coefficients. Then the approximation error is optimal for curvelet and no other sparsifying transform can yield a smaller error with the same number of terms. Therefore, curvelet transform is optimally sparse representation of objects with edges.

In this paper, we take curvelet transform as the sparsifying transform and compare it against two state-of-art sparsifying transforms, namely wavelet transform and total variation. One physical phantom and one in vitro dataset were used for evaluation.

## 2 Materials and methods

A discrete version of the CT scanning process can be described as

$$\boldsymbol{Ax} = \boldsymbol{b} \tag{1}$$

Here $A = (a_{ij})$ is the system matrix representing the projection operator, $\boldsymbol{x}$ = ($x_1$,..., $x_n$) represents the object and $\boldsymbol{b}$ = ($b_1$, ..., $b_m$) is the corresponding projection data. So to reconstruct the object $\boldsymbol{x}$ is to solve the linear system. In our case, the linear system is underdetermined due to the undersampling. There exist infinite solutions. As mentioned above, CS takes sparsity as prior knowledge, which formulates the reconstruction problem as

$$\min_{\boldsymbol{x}} ||\Phi\boldsymbol{x}||_{\mathrm{L1}} \; s.t. \; ||\boldsymbol{Ax} - \boldsymbol{b}||_2^2 < \alpha \tag{2}$$

Here, $\alpha$ stands for the variance of the noise. $\Phi$ is the sparsifying transform. In our work, $\Phi$ is curvelet transform. WR and TVR use wavelet and total variation as the sparsifying transforms. The inequality constraint enforces the data fidelity and the L1 norm term promotes the sparsity. It is well known that the constrained optimization problem (2) can be transformed to an easier unconstrained optimization problem [3]

$$\min_{\boldsymbol{x}} ||\Phi\boldsymbol{x}||_{\mathrm{L1}} + \beta||\boldsymbol{Ax} - \boldsymbol{b}||_2^2 \tag{3}$$

The dimension of (3) is very high. Therefore, we employed the forward-backward splitting method [3] to split (3)) to two sub-optimization problems which are easy to solve.

- *Step 1:* One step of gradient descent method to minimize $||\boldsymbol{Ax} - \boldsymbol{b}||_2^2$
- *Step 2:* Solve the optimization problem $\boldsymbol{x'} = \min ||\boldsymbol{x} - \boldsymbol{v}||_2^2 + \beta||\Phi\boldsymbol{x}||_{\mathrm{L1}}$ ($\boldsymbol{v}$ is calculated from step 1 which is the volume estimation from step 1).

– *Step 3:* Repeat step 1 to step 2 until until L2 norm of the difference of the two neighboring estimate is less than a certain value or the maximum iteration number is reached.

To further speed up the optimization process, the SART reconstruction can be applied at Step 1. When the sparsifying transform $\boldsymbol{\Phi}$ is invertible, a simple soft thresholding operator can be used to solve the objective function in step 2 [8]. The optimal solution of the objective function in Step 2 is:

a) Apply the sparsifying transform $\boldsymbol{\Phi}$ on $\boldsymbol{v}$, $\boldsymbol{x}^a = \boldsymbol{\Phi}\boldsymbol{v}$.
b) Apply the soft thresholding operator

$$x_{\mathrm{i}}^b = S(x_{\mathrm{i}}^a, \beta) = \begin{cases} x_{\mathrm{i}}^a - \beta & x_{\mathrm{i}}^a > \beta \\ 0 & |x_{\mathrm{i}}^a| < \beta \\ x_{\mathrm{i}}^a + \beta & x_{\mathrm{i}}^a < \beta \end{cases} \tag{4}$$

where $S(x_{\mathrm{i}}^a, \beta)$ is the soft thresholding operator. $x_{\mathrm{i}}^b$ is the i-th element of $\boldsymbol{x}^b$ and $x_{\mathrm{i}}^a$ is the i-th element of $\boldsymbol{x}^a$. The soft thresholding operator is applied element wisely on $\boldsymbol{x}^a$ to achieve the optimal solution of the objective function in step 2 [3].
c) Apply the inverse sparsifying transform on the results of step b.

When the sparsifying transform $\boldsymbol{\Phi}$ is not invertible (e.g. total variation), simply soft thresholding operator could not solve the optimization problem in step 2. Several gradient descent steps are applied to solve the optimization problem in step 2. To sum up, the optimization algorithm for the method using invertible sparsifying transforms as the regularizer is:

– *Step 1:* One step of SART to minimize $||\boldsymbol{A}\boldsymbol{x} - \boldsymbol{b}||_2^2$
– *Step 2:* Apply the soft thresholding operator:
  • *Step 2.1:* Apply the sparsifying transform on the result of step 1.
  • *Step 2.2:* Apply the soft thresholding operator using (4).
  • *Step 2.3:* Apply the inverse sparsifying transform on the result of Step 2.2.
– *Step 3:* Repeat step 1 to step 2 until L2 norm of the difference of the two neighboring estimate is less than a certain value or the maximum iteration number is reached.

The optimization algorithm for the method using non-invertible sparsifying transforms as the regularizer is:

– *Step 1:* One step of SART to minimize $||\boldsymbol{A}\boldsymbol{x} - \boldsymbol{b}||_2^2$.
– *Step 2:* Apply $k$ steps of sub-gradient descent method to solve $\min ||\boldsymbol{x} - \boldsymbol{v}||_2^2 + \beta||\boldsymbol{\Phi}_1\boldsymbol{x}||_1$ ($\boldsymbol{v}$ is calculated from step 1 which is the volume estimation from step 1).
– *Step 3:* Repeat step 1 to step 2 until L2 norm of the difference of the two neighboring estimate is less than a certain value or the maximum iteration number is reached.

$k$ in Step 2 is usually a fixed number which can guarantee that the solution of Step 2 is accurately enough. We set $k = 3$ as in [4].

## 3 Results

We evaluate our algorithm on one physical phantom dataset (Siemens Cone-beam Phantom, QRM, Möhrendorf, Germany) and one in vitro dataset. Totally 496 projections within 200 degrees were acquired using a C-arm system (Artis Zeego C-arm systems, Siemens, Forchheim, Germany) for both physical phantom and in vitro dataset. Only 50 and 100 equally spaced projections were used to perform the reconstruction for the physical phantom and for in vitro dataset respectively. The resolution of the projection image is $1248 \times 960$ pixels with a pixel size of $0.31 \times 0.31\ mm^2$. In the experiment, we reconstructed the center slice with the size of $512 \times 512$ pixels. The pixel size is $0.49 \times 0.49\ mm^2$. For further evaluation, we also reconstructed the image using WR and TVR. The parameter setting of all methods were chosen according to that the final reconstructions contain the same level of noise. The noise level was denoted by the

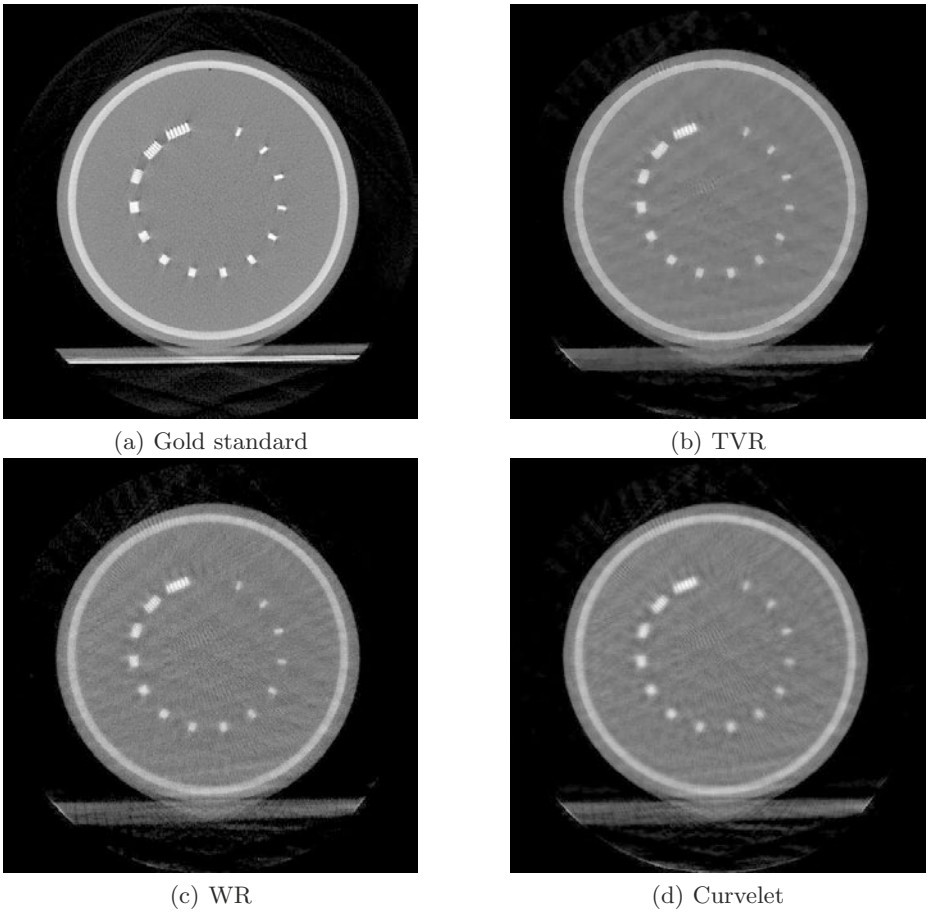

(a) Gold standard (b) TVR

(c) WR (d) Curvelet

**Fig. 1.** Reconstruction results of the physical phantom.

standard derivation of a homogeneous area which is marked with black rectangle in Fig. 1 and Fig. 2. We set parameters in this way because that the datasets used for all methods are the same. Therefore the noise level of the reconstructions should be same. The reconstruction results of the physical phantom are in Fig. 1 and the reconstruction results of in vitro dataset are in Fig. 2. However, TVR introduce the carton-like artifacts. The reconstruction results of WR contains the blocky artifacts (red rectangle in Fig. 2) The reconstruction results of our method do not contain carton-like artifacts.

For qualitative evaluation, we calculated the correlation coefficients of the reconstructions for each method

$$r = \frac{\sum_{\mathrm{n}}(\boldsymbol{x}_{\mathrm{i}} - \bar{\boldsymbol{x}})(\boldsymbol{x}_{\mathrm{i}}^{\mathrm{true}} - \bar{\boldsymbol{x}}^{\mathrm{true}})}{\sqrt{\sum_{\mathrm{n}}(\boldsymbol{x}_{\mathrm{i}} - \bar{\boldsymbol{x}})^2(\boldsymbol{x}_{\mathrm{i}}^{true} - \bar{\boldsymbol{x}}^{\mathrm{true}})^2}} \tag{5}$$

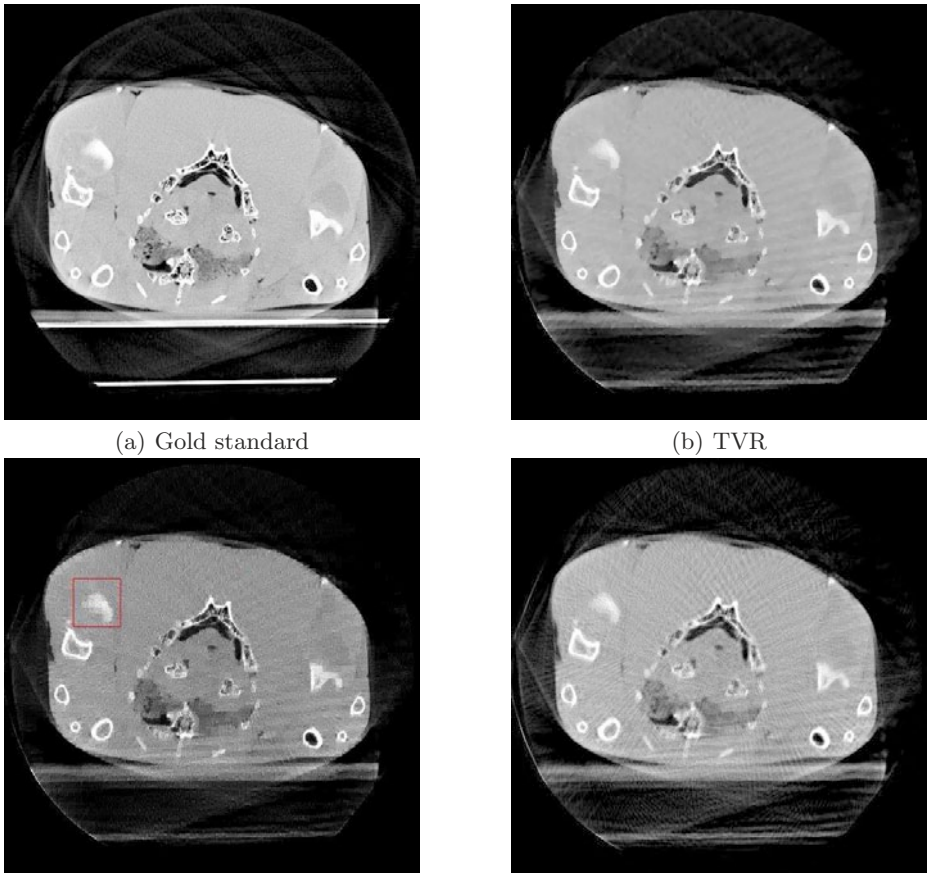

(a) Gold standard (b) TVR

(c) WR (d) Curvelet

**Fig. 2.** Reconstruction results of in vitro dataset.

**Table 1.** Reconstruction error.

| | TVR | WR | Curvelet |
|---|---|---|---|
| Correlation coefficient of physical phantom reconstruction | 96.68% | 96.59% | 96.78% |
| Correlation coefficient of in vitro dataset reconstruction | 94.21% | 93.99% | 94.34% |

$\boldsymbol{x}^{\text{true}}$ is the gold standard which is the image reconstructed by FDK using all projections in our experiments. The results can be found in Tab. 1. The similar conclusion can be drawn. The reconstruction results of our approach is superior to the other methods.

## 4 Discussion

CS uses sparsity as a prior. Therefore, a proper sparse transform is crucial in CS based reconstruction algorithms. Curvelet transform employing directional filter bank is very efficient in encoding images with edges. Often, medical images contain many edges. Therefore, it is quite suitable for CS based reconstruction algorithms. In this work, we introduced the curvelet transform to the CS based reconstruction framework. The experiments show that our approach shows superior image quality compared to the other methods. In addition, since curvelet transform is invertible, the optimization algorithm for our method is simpler than TVR which is the state-of-art CS based reconstruction method.

## References

1. Donoho DL. Compressed sensing. IEEE Trans Inf Theory. 2006;52(4):1289–306.
2. Starck JL, Candès EJ, Donoho DL. The curvelet transform for image denoising. IEEE Trans Image Process. 2002;11(6):670–84.
3. Yu H, Wang G. SART-type image reconstruction from a limia fast and accurate method to solveted number of projections with the sparsity constraint. Int J Biomed Imaging. 2010;2010:3.
4. Sidky EY, Pan X, Reiser IS, et al. Enhanced imaging of microcalcifications in digital breast tomosynthesis through improved image-reconstruction algorithms. Med Phys. 2009;36:4920.
5. Brenner DJ, Hall EJ. Computed tomography: an increasing source of radiation exposure. N Engl J Med. 2007;357(22):2277–84.
6. Wu H, Maier A, Fahrig R, et al. Spatial-temporal total variation regularization (STTVR) for 4D-CT reconstruction. SPIE. 2012;8313:83133J.
7. Starck JL, Candès EJ, Donoho DL. The curvelet transform for image denoising. IEEE Trans Image Process. 2002;11(6):670–84.
8. Donoho DL. De-noising by soft-thresholding. IEEE Trans Inf Theory. 1995;41(3):613–27.